Characterisation of organic inclusions in stalagmites using laser-ablation-micropyrolysis gas chromatography-mass spectrometry

Alison J. Blyth[1,2*], David Fuentes[3], Simon C. George[4], Herbert Volk[3,§]

[1]Department of Environment, Earth & Ecosystems, The Open University, Milton Keynes, MK7 6AA, UK

[2]WA-OIG, Department of Chemistry / The Institute of Geosciences Research, Curtin University, GPO Box U1987, Perth 6845, Western Australia, Australia

[3]CSIRO, PO Box 136, North Ryde, NSW 1670, Australia

[4]Department of Earth and Planetary Sciences, Macquarie University, Sydney, NSW 2109, Australia

[§]Present address: BP Exploration Company, Sunbury-on-Thames, UK

*Corresponding author. Postal address: Department of Applied Geology, Curtin University, Perth, WA 6845, Australia
Email: Alison.Blyth@curtin.edu.au
Tel: +61 8 9266 9388

Abstract

Laser-micropyrolysis gas chromatography-mass spectrometry (La-Py-GC-MS) allows the analysis of small targeted areas of organic material. In this proof of concept study a novel application of the technique is demonstrated. Three types of organic matter preserved in speleothems were analysed: dissolved organic matter within the calcite crystal matrix; detrital organic inclusions; and lithified guano derived from birds and bats. The results indicate that there is significant heterogeneity within each sample type, with guano samples having the highest variability. However, there are also distinctive La-Py-GC-MS products that allow separation of the sample types geochemically. These include the chain length distribution within the longer chain *n*-alkanes (>C_{20}), with the guano sample having a dominance of chain lengths below C_{27}, whilst the other two sample types are dominated by *n*-alkanes of C_{27} and above. The detrital inclusion sample has a higher relative abundance of pyrrole and methylpyrroles. A homologous series of longer chain alkylbenzenes is seen only in the guano samples.

Our preliminary data indicate that fingerprints of La-Py-GC-MS analyses may be useful to provide information on organic matter preserved in speleothems, but more work is required to extend the technique to lower organic content samples, and to fully test the application in a larger dataset of preserved organic matter types.

Keywords

Speleothem; laser micropyrolysis; organic inclusion, gas chromatography-mass spectrometry

1. Introduction

Laser-micropyrolysis gas chromatography-mass spectrometry (La-Py-GC-MS) can yield geochemical information from laser spots as small as ~20 µm spot size, and thus provides the ability to provide reasonably detailed analyses of heterogeneous pyrolysable organic matter at resolutions similar to that of microscopy (Greenwood et al., 1996). In general, La-Py-GC-MS has been demonstrated to provide similar data to flash pyrolysis, but at the 10s of microns scale (Yoshioka and Ishiwatari, 2002), and multiple applications have been developed, especially within organic rich rocks. These include the analysis of individual macerals, so as to ascertain the chemistry specific to each maceral type (Greenwood et al., 1993; Stout, 1993; Greenwood et al., 1998; Greenwood et al., 2001), the characterisation of solid bitumens at the molecular level (Greenwood et al., 2001; Sestak et al., 2009), and the analysis of microfossils, such as Tasmanites algae (Greenwood et al., 1998; Greenwood et al., 2000), acritarchs (Arouri et al., 1999; Arouri et al., 2000), chitinozoans (Jacob et al., 2007) and pollen (Al Sandouk-Lincke et al., 2013). Oil-bearing fluid inclusions have also been analysed by La-Py-GC-MS (Greenwood et al., 1998), although sensitivity and power of the laser tends to lead to some laser artefacts that make comparison with other bulk analytical methods difficult (George et al., 2012). Use of a pulsed femtosecond laser has allowed single oil inclusions to be analysed successfully (Volk et al., 2010). Outside of geology, La-Py-GC-MS has also found use in forensic studies such as analysis of paint flakes (Armitage et al., 2001; Prati et al., 2014). A recent study comparing La-Py-GC-MS to Curie Point Pyrolysis GC-MS (CP-Py-GC-MS) concluded that there were several advantages pertaining to the use of laser pyrolysis, including the provision for smaller sample sizes and good spatial analytical control (Al Sandouk-Lincke et al., 2014), but that the higher (estimated as > 1000 °C) and

68 unquantified temperature applied in laser pyrolysis will affect compound distributions. They
69 therefore concluded that the nature of the organic matter was important in assessing the
70 suitability of pyrolysis techniques, with more mature organic matter better suited to laser
71 work (Al Sandouk-Lincke et al., 2014).
72 Here, a laser pyrolysis instrument with an Nd-YAG infrared laser was used to characterise
73 organic matter preserved within speleothems. The analysis of organic matter in
74 speleothems is a subject of increasing research interest as it potentially provides new
75 palaeoenvironmental records focused on vegetation change (Xie et al., 2003; Blyth et al.,
76 2007; 2011; Rushdi et al. 2011; Li et al., 2014), soil dynamics (Xie et al., 2003; Blyth et al.,
77 2013b; Li et al., 2014), and temperature (Yang et al., 2011; Blyth & Schouten, 2013; Blyth et
78 al., 2014). However, the focus on biomarkers extractable by wet chemistry from the
79 carbonate means that most research to date has required relatively large sample sizes of
80 calcite (1 – 100 g) (Xie et al., 2003; Blyth et al., 2007; Yang et al., 2011; Blyth & Schouten
81 2013; Li et al., 2014), compared to established inorganic geochemical proxies. Selected
82 techniques published to date allow analysis of less than 1 g of calcite: thermochemolysis of
83 lignin (0.5 g; Blyth & Watson, 2009; Blyth et al., 2010); amino acid analysis (25–120 mg,
84 Lauritzen et al., 1998; Blyth et al., 2008); high performance liquid chromatography analysis
85 of short chain fatty acids (0.5–3.5 g, Bosle et al., 2014); and liquid chromatography-isotope
86 ratio mass spectrometry (LC-IRMS) analysis of bulk organic isotopes (0.2 g; Blyth et al.,
87 2013a,b). Of these, only LC-IRMS of bulk $\delta^{13}C$ has so far been fully applied in a multi-proxy
88 palaeoenvironmental reconstruction (Blyth et al., 2013b). The need for larger calcite
89 samples significantly limits the temporal resolution of the time-series recovered, and often
90 excludes the possibility of analysing individual organic inclusions or layers resulting from
91 biofilms or airborne, water-lain, or faunal detrital input. Alternative techniques such as

92 continuous fluorescence analysis have met with good success in providing high resolution
93 records of certain forms of dissolved organic matter (e.g. Baker et al., 1996; Baker et al.,
94 1998; Perrette et al., 2000; Baker & Bolton 2000; Perrette et al., 2005; Baker et al., 2008),
95 but are limited in the amount of molecular detail that can currently be recovered. The
96 development of new analytical techniques that can be applied at a high sample resolution
97 and with minimal wet chemical preparation is therefore desirable.
98 In this paper the La-Py-GC-MS technique was applied to three speleothem samples with
99 contrasting organic contents: (i) soil-derived dissolved organic matter distributed within the
100 crystalline calcite; (ii) detrital or *in-situ* particulate organic matter; and (iii) lithified guano of
101 a known faunal origin. Comparison of these samples and consideration of the characteristic
102 chemical differences provides an initial insight into the potential utility of the La-Py-GC-MS
103 technique, and possible future applications in speleothem geochemistry.
104

105 ## 2. Materials and methods

106 ### 2.1 Samples

107 Three speleothem samples were analysed in this preliminary study to represent three
108 preserved organic matter types. The first is an Australian stalagmite (370 FS03) of Plio-
109 Pleistocene age from the Nullarbor Plain, Australia. This sample has a black colouration
110 hypothesised to be due to a high proportion of humic acids entrapped in the crystalline
111 structure (Caldwell et al., 1982). Due to this abnormal organic content, it is the only
112 speleothem analysed where it was possible to pyrolyse the calcite using the La-Py-GC-MS
113 instrument as currently configured. The second sample is from an Ethiopian stalagmite

(Bero-1) from the Mechara region of Ethiopia, which formed between 10 ka and present in an open cave, recessed into a cliff-face (Asrat et al., 2008). It contains laminae of visible detrital organic matter, which may have been deposited by water, or due to the relatively open nature of the cave, possibly by air or faunal input. The third sample (HV-1) is a crust of lithified guano incorporated into a Peruvian stalagmite from Cueva de las Lechuzas in Peruvian Amazonia, and is believed to be Holocene in age (H. Vonhof pers comm.). Based on modern accumulations in the area, the guano is derived from a mixture of bats and oilbirds, which both live in the cave.

A sample section approximately 5 mm x 5 mm was removed from each speleothem, centring on visible organic inclusions in the case of Bero-1 and HV-1 guano. Prior to analysis, the sample blocks were cleaned in dichloromethane to remove surface contamination. Samples were thermally desorbed in the pyrolysis chamber of the instrument (see Section 2.2) at 100 °C for 10 minutes prior to analysis to reduce desorption artefacts, although the latter were found to be significant only for the guano samples. To minimise these artefacts, piece 2 of the guano was thermally extracted offline at 200 °C, and held at 100 °C in an oven overnight prior to analysis.

2.2 Analytical methods

A detailed description of the instrument and methodology can be found elsewhere (Greenwood et al., 1996; Greenwood et al., 1998; Bernard et al., 2010; Sandouk-Lincke et al., 2013; Prati et al., 2014). Briefly, a continuous wave laser (Laser Applications 9500, Nd:YAG laser, λ= 1064 nm) was tightly focused onto selected areas of the sample through an Olympus BPX60M microscope equipped with reflected light illumination and using long

137 distance working objectives (20X/0.4 and 50X/0.5). The sample was located in a purpose-
138 built pyrolysis chamber (100-110°C, 100 mL helium flow) which was interfaced to a GC-MS
139 system (Hewlett Packard 6890 GC interfaced to a 5973 mass selective detector, electron
140 energy 70eV) via a gas inlet system designed for maximum transfer efficiency of the gaseous
141 products. The products of the pyrolysis process were cryogenically trapped in a coiled nickel
142 loop using a liquid nitrogen bath. After trapping the products, a 6 port transfer valve was
143 rotated to transfer 1 mL/min helium through the trap and the contents were then desorbed
144 by heating to 320 °C. The products were cryo-focused again in a loop of GC column
145 immersed in a liquid nitrogen bath. The full scan GC-MS analysis (m/z 50-550) of the
146 pyrolysates was performed on a DB-5MS column (J&W, 60 m, 0.25 mm I.D., 0.25 µm film
147 thickness) with helium as carrier gas with constant pressure of 25 psi. The GC oven was
148 programmed for an initial temperature of 40 °C (2 min hold) followed by heating at 4 °C/
149 min to 310 °C (30 min hold).
150 The size of the laser crater was controlled by a combination of instrumental parameters
151 such as choosing the appropriate magnification depending on the spatial resolution
152 required for the sample, the laser power and time span of the laser event. The 370 FS03 and
153 Bero-1 stalagmite samples were pyrolysed using a 50x objective and applied power of 19.4
154 W for 1 s or 1.2 W for 0.2 s, respectively, yielding spot sizes of ~20 µm. The lithified guano
155 sample was pyrolysed using a 20x objective and applied power of 1.9 W for 0.2 s, yielding
156 spot sizes of ~40-50 µm. Between 80 and 127 shots into different parts of each sample were
157 aggregated in each run using a liquid nitrogen trap, so as to provide sufficient sensitivity for
158 compound identification. The analytical runs chosen for data analysis are those that
159 produced the largest compound yields for their sample type. Figure 1 shows SEM images of

160 the pyrolysis holes in Bero-1 and HV-1. Compounds were identified by comparison to mass
161 spectral libraries and gas chromatographic retention times (e.g. Eganhouse et al., 1993).
162

163 # 3. Results and discussion

164 ## 3.1 Compounds identified

165 Figure 2 shows representative pyrograms for each of the three sample types, and
166 identified pyrolysis products are listed in Table 1. All the samples contain a homologous
167 series of *n*-alkanes (C_6 – C_{31}), *n*-alkenes (C_6-C_{18}) and a range of low molecular weight
168 aromatic compounds. In addition to the major peaks visible on the TIC pyrogram, other
169 peaks include several compounds of lower abundance that were quantified in some or all of
170 the samples, including o-xylene, *n*-propylbenzene, *iso*-propylbenzene, ethylmethylbenzenes,
171 trimethylbenzenes, methylindenes, pyrrole, methylpyrroles, phenol, a methylphenol, furan,
172 and methylfurans. In terms of organic matter fingerprinting, the main distinguishing
173 considerations to separate the three sample types were found to be the relative proportions
174 of compounds within the *n*-alkane series, and the presence or absence of some key
175 aromatic groups.
176

177 ## 3.2 *n*-Alkenes and *n*-alkanes

178 Homologous series of *n*-alkenes and *n*-alkanes are frequently seen from the pyrolysis of
179 organic matter (Hatcher & Clifford 1994; Fezzey & Armitage, 2006; Al Sandouk-Lincke et al.,
180 2014), deriving from the pyrolysis breakdown of larger biopolymers. Their dominance in a
181 pyrogram has previously been associated with humic acids (Fezzey & Armitage, 2006),

182 although it has also been suggested that this dominance is a result of an inherent analytical
183 bias in favour of non-polar compounds (Hatcher & Clifford 1994). The results here indicate
184 that interrogation of the relative chain length distribution within each group (*n*-alkenes; *n*-
185 alkanes <C_{20}; *n*-alkanes >C_{20}) is informative in partially separating the three sample types.
186 Low and higher molecular weight n-alkanes are discussed separately due to the bimodality
187 of the chromatograms.
188 The *n*-alkene series runs from C_6-C_{18} in Bero-1, C_7-C_{16} in 370 FS03, and C_6-C_{21} in the HV-1
189 guano samples (Fig. 3). Within the alkenes present, there is little variation between repeat
190 analyses of each sample type for Bero-1 and HV-1 (r^2 = 0.90 to 0.98, p = 0.0000). For 370
191 FS03, only one analytical run (370 FS03 brown) produced a series of alkenes, with the
192 second run (370 FS03 black) containing only C_{14} at a measurable abundance. When
193 considering the differences between sample types, the Bero-1 detritus and HV-1 guano
194 show a significant correlation (Fig. 4a; r^2 = 0.83, p = 0.0000), with decreasing abundance
195 with increasing chain length. In contrast the organic matter coating the crystals in 370 FS03
196 does not correlate with either of the other sample types, having a reduced number of
197 measurable alkenes, and three distinct maxima at C_8, C_{14}, and C_{16}.
198 For *n*-alkanes, different distributions and relationships are apparent between the three
199 sample types in both the low molecular weight (LMW, chain length C_{19} and below) and high
200 molecular weight (HMW, chain length C_{20} and above) components. Fig. 5 shows the LMW
201 groups. Variation within each sample type is greater than for the *n*-alkenes. Repeat analyses
202 for Bero-1 show a significant correlation (r^2 = 0.73, p < 0.0001), as do the two repeats on HV-
203 1 piece 2 (r^2 = 0.67, p < 0.0005). However, there is no meaningful relationship between HV-1
204 piece 2 and HV-1 piece 1 (r^2 = 0.16, p > 0.1). This difference is most likely down to the
205 increased pre-extraction for piece 2, with piece 1 still showing alkane artefacts from

206 desorption. There is also no meaningful correlation between the two analyses of 370 FS03
207 (r^2 = 0.06, p > 0.1), partly because one repeat (370 FS03 black) did not contain measurable
208 alkanes at the lower end of the chain length range. However, the overall trend in this
209 sample, *n*-alkanes increasing in abundance with increasing chain length, is similar for both
210 analyses, and is contrary to that in Bero-1 and HV-1, both of which have a decrease in *n*-
211 alkane abundance with increasing chain length, but with different patterns. Therefore, as for
212 the *n*-alkenes, LMW *n*-alkanes seem most useful in separating 370 FS03 from the other two
213 sample types, based on the trend of the inverse correlations (Fig. 4b). It is not certain at
214 present why the *n*-alkanes and *n*-alkenes exhibit different chain length patterns in these
215 results, and this is an issue that merits further research before definite environmental
216 interpretations are developed from this approach.
217 The HMW group shows more distinct and useful patterns. In particular, the dominant
218 chain length in the distribution is different in each sample type, and consistent between
219 analyses of the same sample type, regardless of other variations in the composition. Bero-1
220 shows a maximum at C_{29}, 370 FS03 at C_{27}, and HV-1 at C_{23} (Fig. 6). Over the whole
221 distribution there is very little variation between the two Bero-1 runs (r^2 = 0.95, p = 0.0000).
222 In the HV-1 guano samples, the two runs of piece 2 also have a good correlation (r^2 = 0.79, p
223 < 0.0001), but the relationship between the two pieces is much less significant (r^2 = 0.53, p <
224 0.1). The two runs of 370 FS03 also have a relatively weak correlation (r^2 = 0.53, p < 0.1).
225 When the average relative distributions are compared between sample type, there is a
226 reasonable correlation between Bero-1 and 370-FS03 (r^2 = 0.70, p < 0.001), but not between
227 either of these and HV-1. This is clearly shown in the % chart in Figure 7, where it can be
228 seen that the HV-1 guano is dominated by chain lengths between C_{20} and C_{23}, whereas the
229 Bero-1 detritus and 370-FS03 organic matter are dominated by C_{27}-C_{31}.

3.3 Other compounds

A number of compound groups have been identified as being significant in natural organic matter pyrolysis, including phenols, pyrroles, furans, and aromatic hydrocarbon precursors such as indenes, methylbenzenes and naphthalenes (e.g. Wilson et al., 1983; White et al., 2007). The relative abundance of these fractions has previously been suggested as a method of discriminating between organic matter types in soils (White et al., 2007). However, in this study, although there are some bulk differences between the three sample types (Fig 8a), there are also good correlations, with *p* values under 0.05 (Fig 8b). This result suggests that for these three samples, using this technique, the relative abundance of the compounds listed above is not a good discriminator. However, two compound groups do stand out as different. The pyrroles (nitrogen compounds most likely derived from proteins; Wilson et al., 1983), have a much higher relative abundance in the Bero-1 detritus (Fig. 8), and a set of longer-chain alkylbenzenes only occur in the HV-1 guano (Fig. 9). The presence of only a single isomer at each carbon number for these alkylbenzenes indicates a natural source (Takada & Ishiwatari 1989). The guano samples did not contain any of the compounds previously identified as diagnostic pyrolysis markers for chitin (e.g. acetylpyridones, acetamidofuran, etc; see Stankiewicz et al., 1996), indicating that the guano may not have been derived from an insectivorous source, although further work on modern cave guano samples would be required to demonstrate this.

3.4 Future research directions

Overall the results of this study indicate some intriguing differences between the three sample types, but caution also needs to be applied in designating a parameter as due to source organic matter variations, as some parameters (e.g. alkane chain length) have been shown to have a relationship with pyrolysis temperature (Al Sandouk-Lincke et al., 2014). Although laser pyrolysis temperatures will be uniformly high, they are not controlled as exactly as in other pyrolysis techniques, which means the precise range of pyrolysis temperatures applied here cannot be quantified. The data here are preliminary, and the abundances of compounds measured is relatively low, so the sample range is not at this stage sufficient to provide definitive identifications of the source of organic matter inclusions in time-series records.

A limitation on this technique is the applicability only to speleothem samples with discrete organic inclusions or a high visible organic content within the crystal matrix. The early stage of this research trialled the technique on speleothems without visible organic contents, but no data was recoverable, as the laser was not sufficient to pyrolyse the calcite. Experimentation with the technique using alternate laser sources is therefore indicated to attempt to expand the applicability, as this approach would be of particular potential use in characterising organic matter at laminae level resolutions which are too small to be feasible to study via the conventional wet chemistry methods currently used on speleothems. Such a study would also be able to investigate the effect of calcite type and texture on organic matter ablation.

A final issue that would benefit from further research is that of potential contamination, as a recent study published after the completion of the experimental phase of this research has suggested that some molecules in speleothem extractions may be

artefacts due to contamination (Wynn & Brocks 2014). The 2014 study only dealt with a limited suite of biomarkers within speleothems, and not the organic inclusions and macromolecules analysed in this paper. Precautions were taken in this work by solvent cleaning and thermal desorption prior to laser pyrolysis to maximise the integrity of the data. However, there is certainly scope for further research to consider the potential changes in pyrolysis products with depth from the cut surface within a single inclusion or laminae, and whether any such changes may relate to contamination or natural heterogeneity.

4. Conclusions

- The Peruvian guano (HV-1) has two distinguishing features separating it from both the other sample types: the dominance of the lower carbon numbers in the long chain (>C_{20}) *n*-alkanes, and the presence of longer chain alkylbenzenes. These features are consistent between both guano pieces, despite some other differences in composition.
- The detrital inclusions in the Ethiopian sample Bero-1 contain higher proportions of furans, pyrroles and phenols than the other samples.
- The DOM in the black Nullarbor Plain speleothem 370 FS03 differed from the other samples in the trends of the *n*-alkenes and shorter chain *n*-alkanes, and in the smaller range of aromatic and nitrogen compounds. This is consistent with the proposed dominance of humic acids as the cause for the colouration in these samples (Caldwell 1982), in the light of some research on pyrolysis of humic acids (Fezzey & Armitage 2006). However, the absence of some compounds may be a

function of the low abundance of pyrolysable material in the sample, rather than in the nature of that material, meaning that a direct comparison with other OM types must be approached with caution.

- The results indicate that La-Py-GCMS may have the potential to characterise detrital organic matter in speleothems, and further work on a greater range of samples, and with alternative laser set-ups to allow the pyrolysis of the calcite is indicated to test the true applicability of this approach

Acknowledgements

Some aspects of this work were supported by ARC DP0985214, and NERC grant NE/G016925/1, HG A3897. AJB acknowledges a Leverhulme Early Career Fellowship held at the Open University. Curtin University and an AINSE Research Fellowship to AJB are also acknowledged for support during final data analysis. Bero-1 was loaned by Andy Baker of the University of New South Wales, and collected by Asfawossen Asrat of Addis Ababa University. 370 FS03 was supplied and dated by Jon Woodhead of the University of Melbourne under ARC DP0985214. HV-1 was collected and supplied by Hubert Vonhof of Vrij University, Amsterdam. All sample owners are thanked for their contribution.

References

Al Sandouk-Lincke, N.A., Schwarzbauer, J., Volk, H., Hartkopf-Froder, C., Fuentes, D., Young, M., Littke, R., 2013. Alteration of organic material during maturation: A pyrolytic and

infrared spectroscopic study of isolated bisaccate pollen and total organic matter (Lower Jurassic, Hils Syncline, Germany). Organic Geochemistry 59, 22-36.

Al Sandouk-Lincke, N.A., Schwarzbauer, J., Hartkopf-Fröder, C., Volk, H., Fuentes, D., Young, M., Littke, R. 2014. The effect of different pyrolysis temperatures on organic microfossils, vitrain and amber - a comparative study between laser assisted- and Curie Point-pyrolysis-gas chromatography/mass spectrometry. Journal of Analytical and Applied Pyrolysis 107, 211-223.

Armitage, S., Saywell, S.S., Roux, C., Lennard, C., Greenwood, P., 2001. The analysis of forensic samples using laser micro-pyrolysis gas chromatography mass spectrometry. Journal of Forensic Science 46, 1043–1052.

Arouri, K., Greenwood, P.F., Walter, M.R., 1999. A possible chlorophycean affinity of some Neoproterozoic acritarchs. Organic Geochemistry 30, 1323-1337.

Arouri, K.R., Greenwood, P.F., Walter, M.R., 2000. Biological affinities of Neoproterozoic acritarchs from Australia: microscopic and chemical characterisation. Organic Geochemistry 31, 75-89.

Asrat, A., Baker, A., Leng, M.J., Gunn, J., Umer, M. 2008. Environmental monitoring in the Mechara caves, Southeastern Ethiopia: implications for speleothem palaeoclimatic studies. International Journal of Speleology 37, 207-220.

Baker, A., Barnes, W.L., Smart, P.L., 1996. Speleothem luminescence intensity and spectral characteristics: signal calibration and a record of palaeovegetation change. Chemical Geology 130, 65–76.

Baker, A., Genty, D., Smart, P.L., 1998. High-resolution records of soil humification and palaeoclimate change from speleothem luminescence excitation and emission wavelength variations. Geology 26, 903–906.

343 Baker, A., Bolton, L., 2000. Speleothem organic acid luminescence intensity ratios: a new
344 palaeoenvironmental proxy. Cave and Karst Science 27, 121–124.
345 Baker, A., Smith, C.L., Jex, C., Fairchild, I.J., Genty, D., Fuller, L. 2008. Annually laminated
346 speleothems: a review. International Journal of Speleology 37, 193-206.
347 Bernard, S., Horsfield, B., Schulz, H-M., Schreiber, A., Wirth, R., Anh V., Tiem T., Perssen, F.,
348 Koenitzer, S., Volk, H., Sherwood, N., Fuentes, D. 2010. Multi-scale detection of
349 organic and inorganic signatures provides insights into gas shale properties and
350 evolution. Chemie der Erde. 70(S3):119-133.
351 Blyth, A.J. & Watson J.S., 2009. Thermochemolysis of organic matter preserved in
352 stalagmites: a preliminary study. Organic Geochemistry, 40, 1029-1031.
353 Blyth, A.J., Schouten, S., 2013. Calibrating the glycerol dialkyl glycerol tetraether signal in
354 speleothems. Geochimica et Cosmochimica Acta 109, 312–328.
355 Blyth, A.J., Asrat, A., Baker, A., Gulliver, P., Leng, M., Genty, D., 2007. A new approach to
356 detecting vegetation and land-use change: high resolution lipid biomarker records in
357 stalagmites. Quaternary Research 68, 314–324.
358 Blyth, A.J., Baker, A., Penkman, K.E.H., Collins, M.J., Gilmour, M.A., Moss, J.S., Genty, D. &
359 Drysdale, R. 2008. Molecular organic matter in speleothems as an environmental
360 proxy. Quaternary Science Reviews, 27, 905-921
361 Blyth A.J., Watson, J.S., Woodhead, J. & Hellstrom, J. 2010. Organic compounds preserved in
362 a three million year old stalagmite from the Nullarbor Plain, Australia. Chemical
363 Geology 279, 101-105.
364 Blyth, A.J., Baker, A., Thomas, L.E., van Calsteren, P., 2011. A 2000-year lipid biomarker
365 record preserved in a stalagmite from northwest Scotland. Journal of Quaternary
366 Science 26, 326–334.

Blyth, A.J., Shutova, Y., Smith, C.I. 2013a. $\delta^{13}C$ analysis of bulk organic matter in speleothems using liquid chromatography–isotope ratio mass spectrometry. Organic Geochemistry 55, 22-25.

Blyth, A.J., Smith, C.I., Drysdale, R.N., 2013b. A new perspective on the $\delta^{13}C$ signal preserved in speleothems using LC-IRMS analysis of bulk organic matter and compound specific stable isotope analysis. Quaternary Science Reviews 75,143–149.

Blyth, A.J., Jex, C.N., Baker, A., Khan, S., Schouten, S. 2014. Contrasting distributions of glycerol dialkyl glycerol tetraethers (GDGTs) in speleothems and associated soils. Organic Geochemistry 69, 1-10

Bosle, J.M., Mischel, S.A., Schulze, A.L., Scholz, D. Hoffmann, T. 2014. Quantification of low molecular weight fatty acids in cave drip water and speleothems using HPLC-ESI-IT/MS - development and validation of a selective method. Analytical and Bioanalytical Chemistry DOI: 10.1007/s00216-014-7743-6.

Caldwell, J., Davey, A.G., Jennings, G.N., Spate, A.P., 1982. Colour in some Nullarbor Plain speleothems. Helictite 20, 3–10.

Eganhouse, R.P, Dorsey, T.F., Phinney, C.S., Westcott, A.M., 1993. Determination of C_6–C_{10} aromatic hydrocarbons in water by purge-and-trap capillary gas chromatography. Journal of Chromatography 628, 81-92.

Fezzey, S., Armitage, R.A. 2006. Pyrolysis GC-MS and THM-GC-MS studies of a black coating from Little Lost River Cave, Idaho. Journal of Analytical and Applied Pyrolysis 77, 102-110.

George, S.C., Volk, H., Dutkiewicz, A., 2012. Mass Spectrometry Techniques for Analysis of Oil and Gas Trapped in Fluid Inclusions, in: Lee, M.S. (Ed.), Handbook of Mass Spectrometry. Wiley, pp. 647-673.

391 Greenwood, P.F., Zhang, E., Vastola, F.J., Hatcher, P.G., 1993. Laser Micropyrolysis Gas-
392 Chromatography Mass-Spectrometry of Coal. Analytical Chemistry 65, 1937-1946.
393 Greenwood, P.F., George, S.C., Wilson, M.A., Hall, K.J., 1996. A new apparatus for laser
394 micropyrolysis-gas chromatography/mass spectrometry. Journal of Analytical and
395 Applied Pyrolysis 38, 101-118.
396 Greenwood, P.F., George, S.C., Hall, K., 1998. Applications of laser micropyrolysis gas
397 chromatography mass spectrometry. Organic Geochemistry 29, 1075-1089.
398 Greenwood, P.F., Arouri, K.R., George, S.C., 2000. Tricyclic terpenoid composition of
399 Tasmanites kerogen as determined by pyrolysis GC-MS. Geochimica et
400 Cosmochimica Acta 64, 1249-1263.
401 Greenwood, P.F., George, S.C., Pickel, W., Zhu, Y.M., Zhong, N.N., 2001. In situ analytical
402 pyrolysis of coal macerals and solid bitumens by laser micropyrolysis GC-MS. Journal
403 of Analytical and Applied Pyrolysis 58, 237-253.
404 Greenwood, P.F., van Heemst, J.D.H., Guthrie, E.A., Hatcher, P.G., 2002. Laser micropyrolysis
405 GC-MS of lignin. Journal of Analytical and Applied Pyrolysis 62, 365-373.
406 Greenwood, P.F., 2011. Lasers used in analytical micropyrolysis. Journal of Analytical and
407 Applied Pyrolysis 92, 426-429.
408 Hatcher, P.G., Clifford, D.J. 1994. Flash pyrolysis and in situ methylation of humic acids from
409 soil. Organic Geochemistry 21, 1081-1092.
410 Jacob, J., Paris, F., Monod, O., Miller, M.A., Tang, P., George, S.C., Beny, J.M., 2007. New
411 insights into the chemical composition of chitinozoans. Organic Geochemistry 38,
412 1782-1788.
413 Lauritzen, S.E., Haugen, J.E., Lovlie, R., Giljenielsen, H. 1994. Geochronological potential of
414 Isoleucine epimerization in calcite speleothems. Quaternary Research 41, 52-58.

Li, X., Hi, C., Huang , J., Xie, S., Baker, A. 2014. A 9000-year carbon isotopic record of acid-soluble organic matter in a stalagmite from Heshang Cave, central China: Palaeoclimate implications. Chemical Geology 388, 71-77.

Perrette, Y., Delannoy, J-J., Bolvin, H., Cordonnier, M., Destombes, J.L., Zhilinskaya, E.A., Aboukais, A. 2000. Comparative study of a stalagmite sample by stratigraphy, laser induced fluorescence spectroscopy, EPR spectrometry and reflectance imaging. Chemical Geology 162, 221-243.

Perrette, Y., Delannoy, J-J., Desmet, M., Lignier, V., Destombes, J.L. 2005. Speleothem organic matter content imaging. The use of a Fluorescence Index to characterise the maximum emission wavelength. Chemical Geology 214, 193-208.

Prati, S., Fuentes, D., Sciutto, G., Mazzeo, R., 2014. The use of laser pyrolysis-GC-MS for the analysis of paint cross sections. Journal of Analytical and Applied Pyrolysis 105, 327-334.

Rushdi, A.I., Clark, P.U., Mix, A.C., Ersek, V., Simoneit, B.R.T., Cheng, H., Edwards, R.L 2011. Composition and sources of lipid compounds in speleothem calcite from southwestern Oregon and their palaeoenvironmental implications. Environmental Earth Sciences 62, 1245-1261.

Sestak, S., Singh, V., Volk, H., George, S.C., Dutkiewicz, A., 2009. Pyrolysis of Jamison Sandstone solid bitumen from the Mesoproterozoic Roper Superbasin. Journal of Geochemical Exploration 101, 94.

Stankiewicz, B.A., van Bergen, P.F., Duncan, I.J., Carter, J.F., Briggs, D.E.G., Evershed, R.P. 1996. Recognition of chitin and proteins in invertebrate cuticles using analytical pyrolysis / gas chromatography and pyrolysis gas chromatography mass spectrometry. Rapid Communications in Mass Spectrometry 10, 1747-1757.

Stankiewicz, B.A., Briggs, D.E.G., Evershed, R.P. 1997. Chemical composition of Palaeozoic and Mesozoic fossil invertebrate cuticles as revealed by pyrolysis-gas chromatography / mass spectrometry. Energy and Fuels 11, 515-521.

Stout, S.A., 1993. Lasers in organic petrology and organic geochemistry. 2. In-situ laser micropyrolysis GCMS of coal macerals. International Journal of Coal Geology 24, 309-331.

Takada, H., Ishiwatari, R. 1989. Biodegradation experiments of linear alkylbenzenes (LABs): Isomeric composition of C_{12} LABs as an indicator of the degree of LAB degradation in the aquatic environment. Environmental Science and Technology 24, 86-91.

Volk, H., Fuentes, D., Fuerbach, A., Miese, C., Koehler, W., Bärsch, N., Barcikowski, S., 2010. First on-line analysis of petroleum from single inclusion using ultrafast laser ablation. Organic Geochemistry 41, 74-77.

White, D.M., Hodkinson, I.D., Seelen, S.J., Coulson. S.J. 2007. Characterization of soil carbon from a Svalbard glacier-retreat chronosequence using pyrolysis-GC/MS analysis. Journal of Analytical and Applied Pyrolysis 78, 70-75.

Wilson, M.A., Philip, R.P., Gillam, A.H., Gilbert, T.D., Tate, K.R. 1983. Comparison of the structure of humic substances from aquatic and terrestrial sources by pyrolysis gas chromatography-mass spectrometry. Geochmica et Cosmochimica Acta 47, 497-502.

Wynn, P.M., Brocks, J.J. 2014. A framework for the extraction and interpretation of organic molecules in speleothem carbonate. Rapid Communications in Mass Spectrometry 28, 845-854.

Xie, S., YI, Y., Huang, J., Hu, C., Cai, Y., Collins, M., Baker, A., 2003. Lipid distribution in a subtropical southern China stalagmite as a record of soil ecosystem response to palaeoclimate change. Quaternary Research 60, 340–347.

463 Yang, H., Ding, W., Zhang, C.L., Wu, X., Ma, X., He, G., Huang, J., Xie, S., 2011. Occurrence of
464 tetraether lipids in stalagmites: implications for sources and GDGT-based proxies.
465 Organic Geochemistry 42, 108–115.
466 Yoshioka, H., Ishiwatari, R., 2002. Characterization of organic matter generated from Green
467 River shale by infrared laser pyrolysis. Geochemical Journal 36, 73-82.
468 Zhang, Z.R., Greenwood, P., Zhang, Q., Rao, D., Shi, W.J., 2012. Laser ablation GC-MS
469 analysis of oil-bearing fluid inclusions in petroleum reservoir rocks. Organic
470 Geochemistry 43, 20-25.
471
472

473 Table and Figure captions

474 Table 1. List of identified and quantified compounds
475 Figure 1. SEM images showing laser ablation holes (indicated with arrow) in a) a detrital
476 inclusion in Bero-1, and b) the lithified guano of HV-1.
477 Figure 2. Total ion chromatograms of La-Py-GC-MS analyses of a) Bero-1 debris run 1; b) 370
478 FS03 brown; c) HV-1 p2. 127 shots. Compound identifications are provided in Table
479 1.
480 Figure 3. Distribution of carbon chain lengths of *n*-alkenes in a) Bero-1 debris; b) 370 FS03; c)
481 HV-1. Scatter plots show the level of correlation between runs within each sample
482 type. C_{11} is excluded from HV-1 piece 1, as it co-eluted with alkane desorption
483 artefacts.
484 Figure 4. Scatter plots showing the correlations between sample types for a) *n*-alkenes; b)
485 shorter chain *n*-alkanes ($<C_{20}$); c) longer chain *n*-alkanes ($>C_{20}$)

Figure 5. Distribution of carbon chain lengths of shorter chain n-alkanes ($<C_{20}$) in a) Bero-1 debris; b) 370 FS03; c) HV-1. Scatter plots show the level of correlation between runs within each sample type. C_{11} is excluded from HV-1 piece 1, as it co-eluted with alkane desorption artefacts.

Figure 6. Distribution of carbon chain lengths of longer chain *n*-alkanes in a) Bero-1 debris; b) 370 FS03; c) HV-1. Scatter plots show the level of correlation between runs within each sample type.

Figure 7. A percentage bar chart showing the increased dominance of compounds below C_{25} in HV-1 in comparison to increased longer chain compounds in Bero-1 and 370 FS03.

Figure 8. a) Pie charts showing the average relative abundances of aromatic compounds within each sample type. Pyrroles are a major feature of Bero-1. b) Scatter plots showing the correlation between the different sample types for the aromatic compounds.

Figure 9. A percentage bar chart of propyl-, methyl- and alkyl benzenes in the three sample types, showing the presence of longer chain alkyl benzenes in HV-1 only.

Figure 1

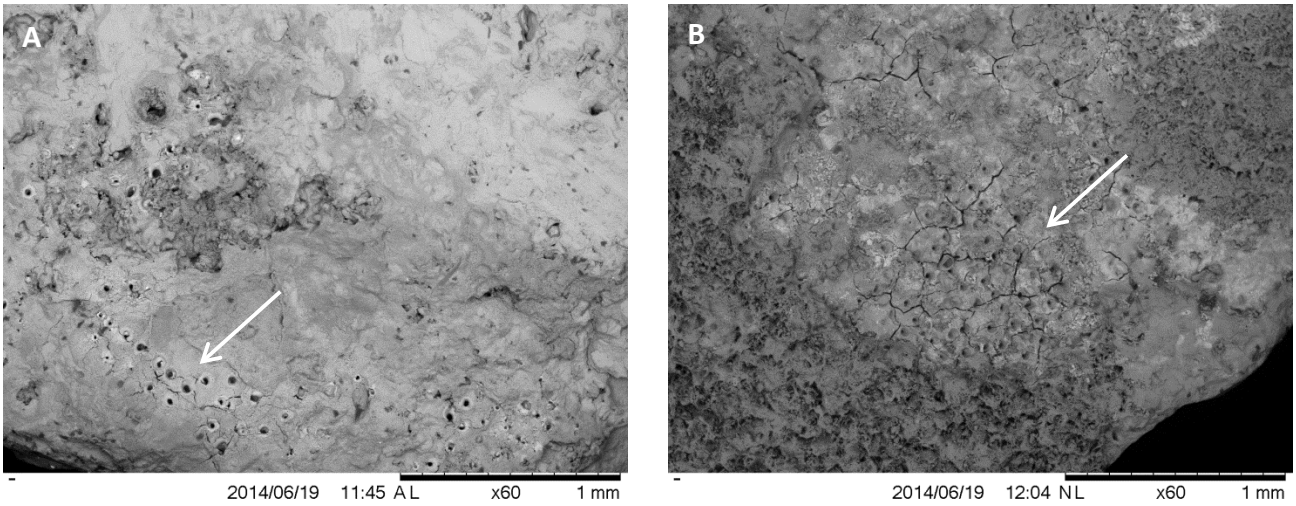

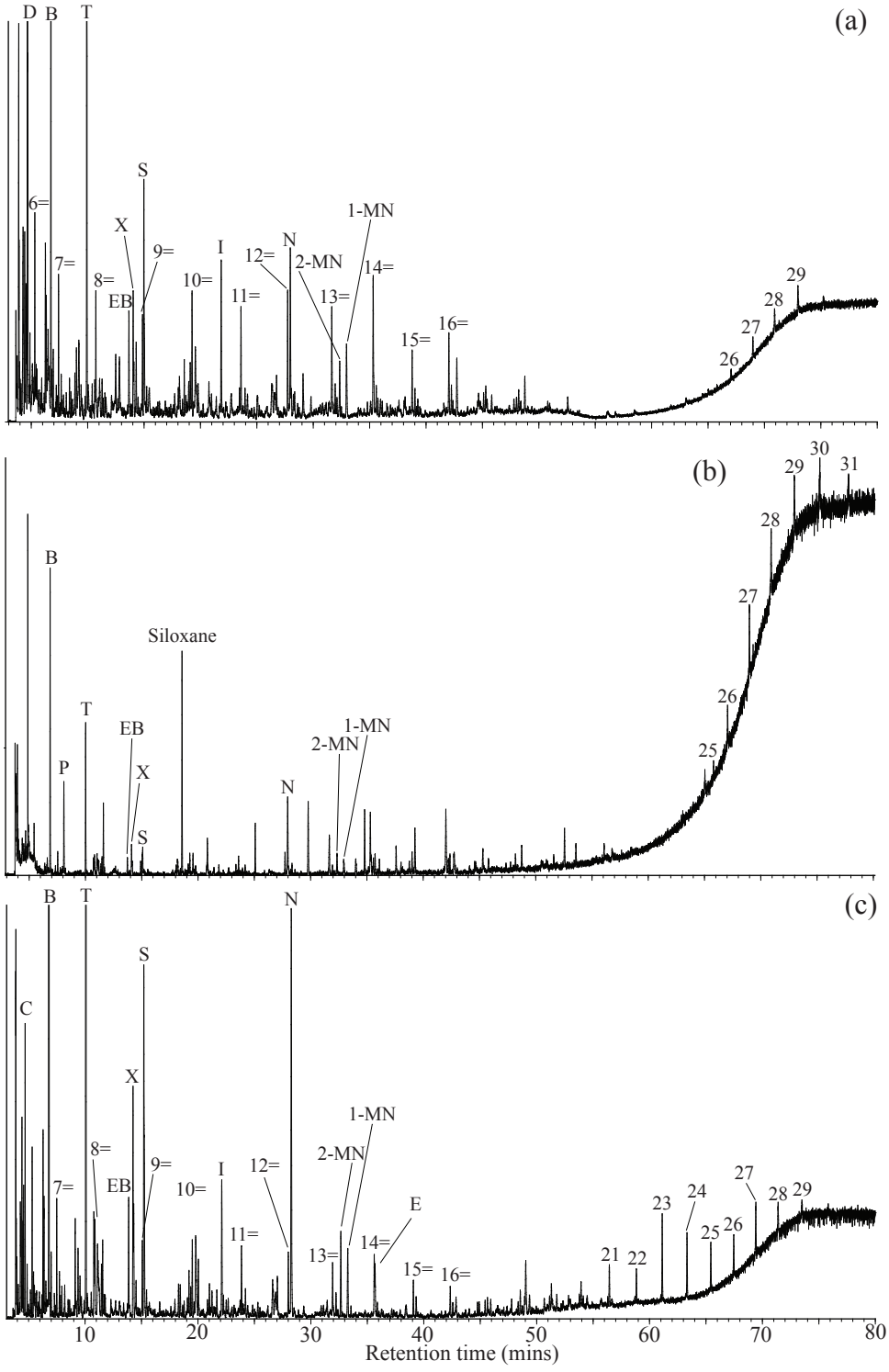
(a)
D
B
T
S
6=
X
9=
I
12=
N
1-MN
2-MN
14=
7=
8=
EB
10=
11=
13=
15=
16=
26
27
28
29
(b)
29
30
31
28
B
27
Siloxane
26
T
EB
1-MN
2-MN
P
X
25
N
S
(c)
B
T
N
S
C
X
1-MN
8=
2-MN
9=
I
12=
7=
EB
10=
E
23
24
27
11=
14=
25
26
28
29
13=
21
22
15=
16=
10
20
30
40
50
60
70
80
Retention time (mins)

Figure 3.

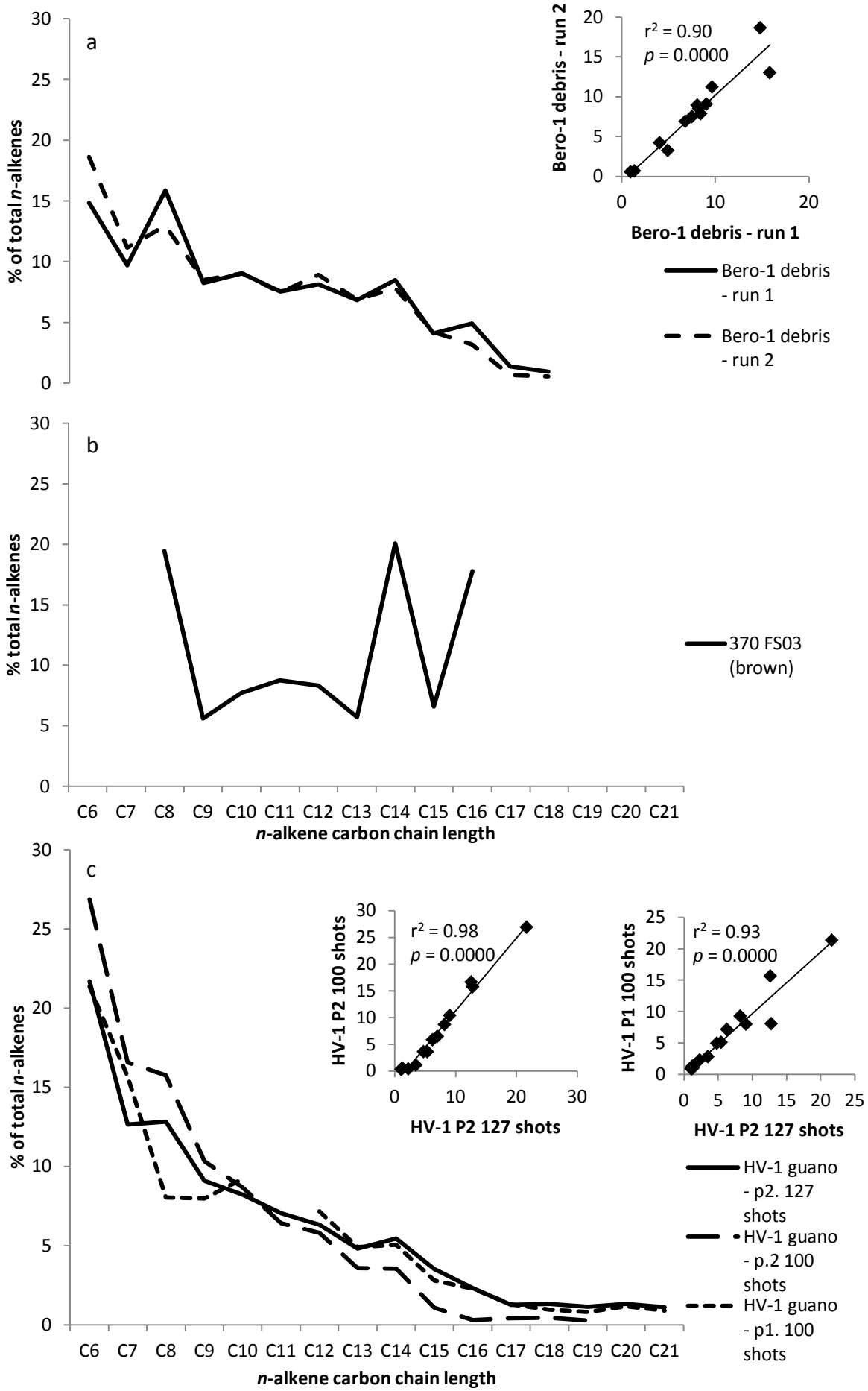
a
% of total n-alkenes
Bero-1 debris - run 2
Bero-1 debris - run 1
r² = 0.90
p = 0.0000
Bero-1 debris - run 1
Bero-1 debris - run 1
Bero-1 debris - run 2
b
% total n-alkenes
370 FS03 (brown)
C6 C7 C8 C9 C10 C11 C12 C13 C14 C15 C16 C17 C18 C19 C20 C21
n-alkene carbon chain length
c
% of total n-alkenes
HV-1 P2 100 shots
r² = 0.98
p = 0.0000
HV-1 P2 127 shots
HV-1 P1 100 shots
r² = 0.93
p = 0.0000
HV-1 P2 127 shots
HV-1 guano - p2. 127 shots
HV-1 guano - p.2 100 shots
HV-1 guano - p1. 100 shots
C6 C7 C8 C9 C10 C11 C12 C13 C14 C15 C16 C17 C18 C19 C20 C21
n-alkene carbon chain length

a) *n*-alkenes

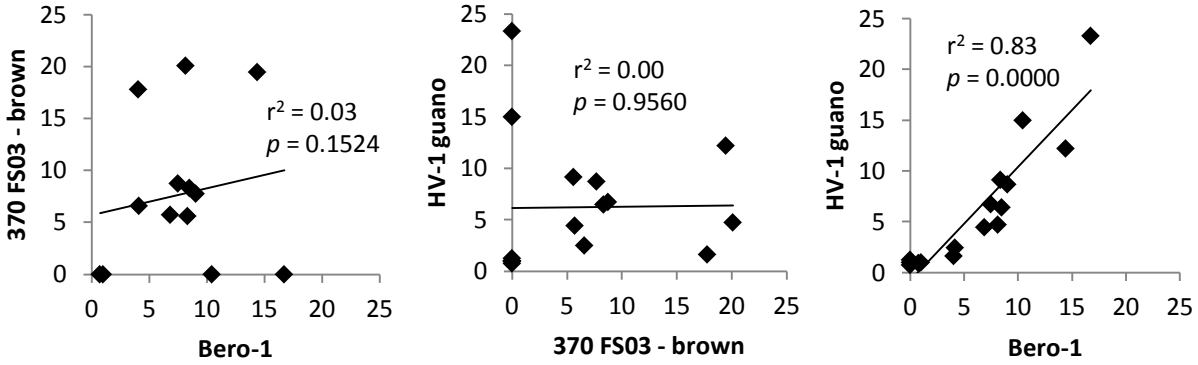

b) *n*-alkanes <C_{20}

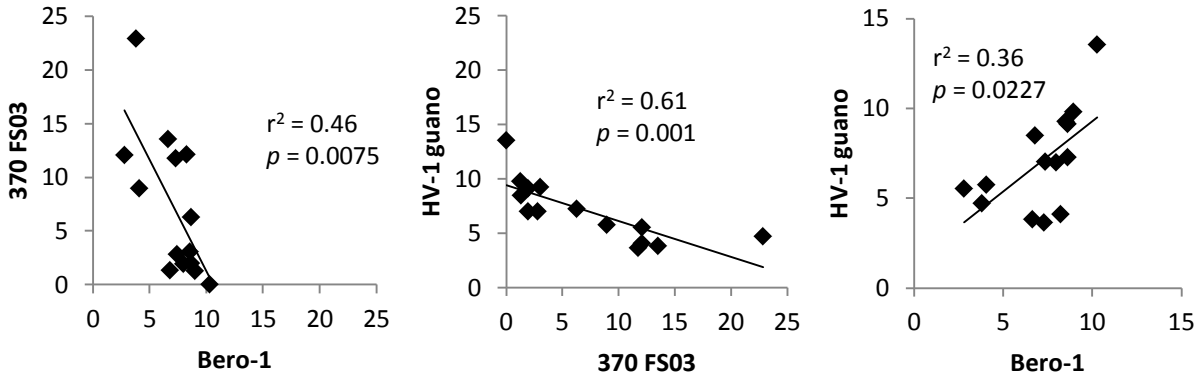

c) *n*-alkanes >C_{20}

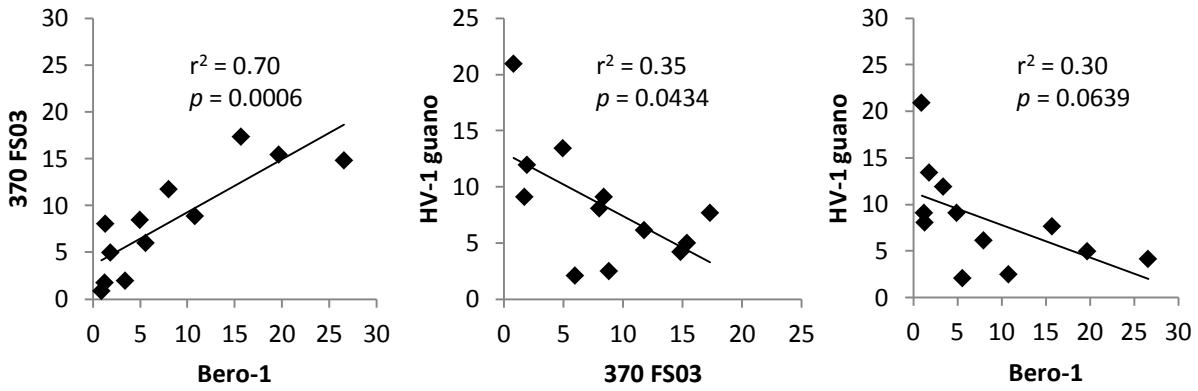

Figure 4.

Figure 5.

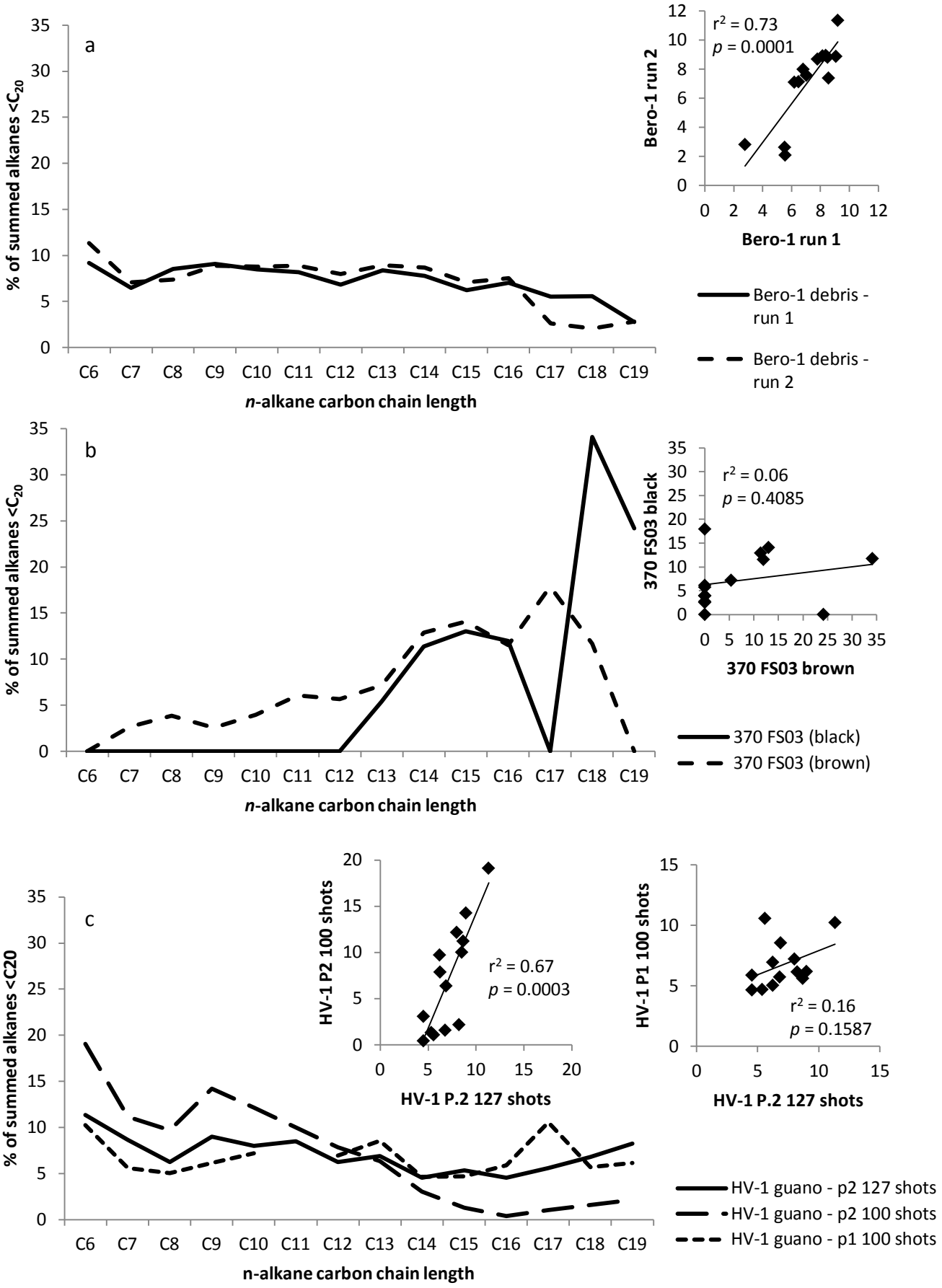
a
% of summed alkanes <C20
n-alkane carbon chain length
C6 C7 C8 C9 C10 C11 C12 C13 C14 C15 C16 C17 C18 C19
r2 = 0.73
p = 0.0001
Bero-1 run 2
Bero-1 run 1
Bero-1 debris - run 1
Bero-1 debris - run 2
b
% of summed alkanes <C20
n-alkane carbon chain length
r2 = 0.06
p = 0.4085
370 FS03 black
370 FS03 brown
370 FS03 (black)
370 FS03 (brown)
c
% of summed alkanes <C20
n-alkane carbon chain length
r2 = 0.67
p = 0.0003
HV-1 P2 100 shots
HV-1 P.2 127 shots
r2 = 0.16
p = 0.1587
HV-1 P1 100 shots
HV-1 P.2 127 shots
HV-1 guano - p2 127 shots
HV-1 guano - p2 100 shots
HV-1 guano - p1 100 shots

Figure 6.

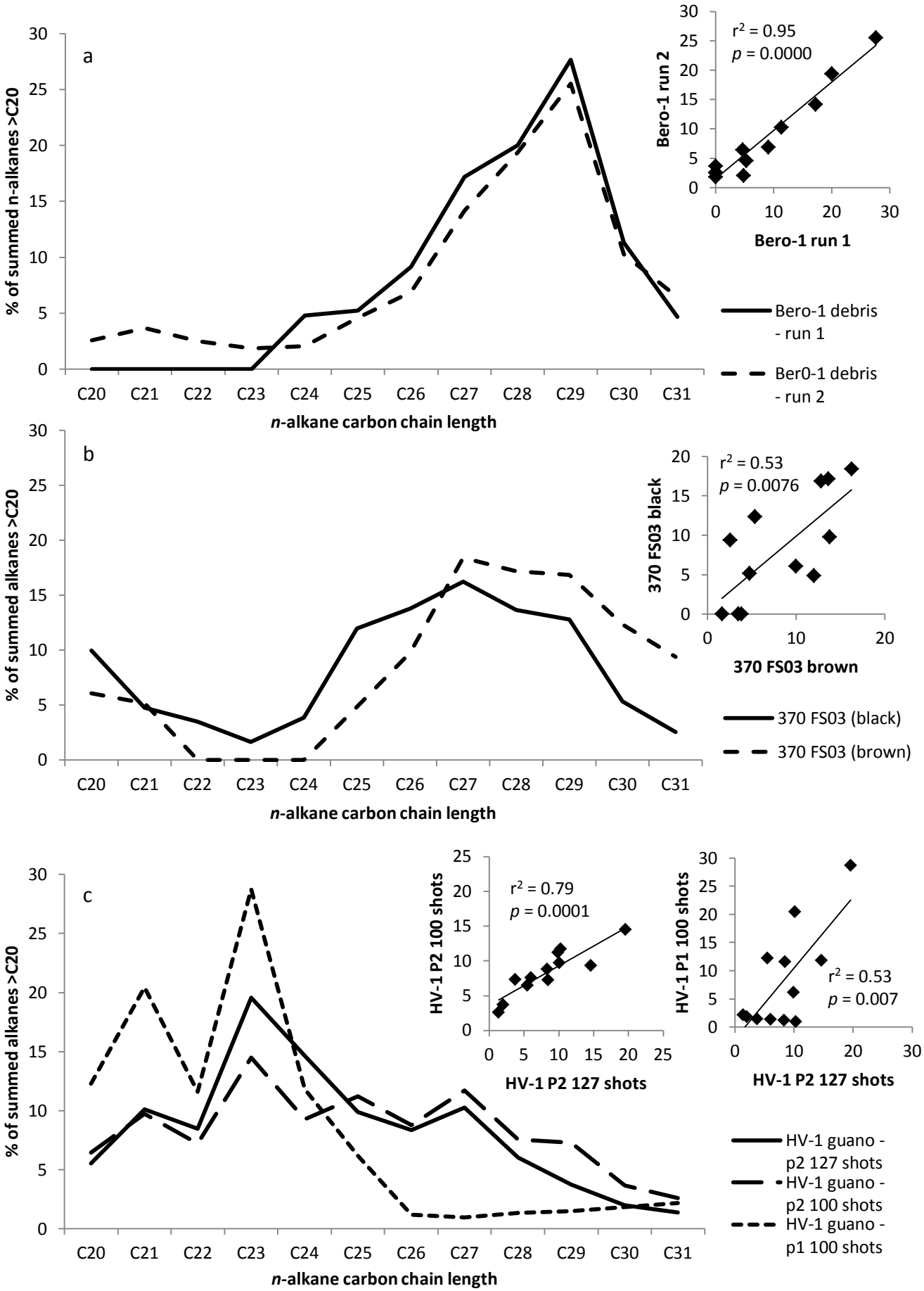
a
% of summed n-alkanes >C20
n-alkane carbon chain length
C20 C21 C22 C23 C24 C25 C26 C27 C28 C29 C30 C31
Bero-1 debris - run 1
Ber0-1 debris - run 2
r² = 0.95
p = 0.0000
Bero-1 run 2
Bero-1 run 1
b
% of summed alkanes >C20
n-alkane carbon chain length
370 FS03 (black)
370 FS03 (brown)
r² = 0.53
p = 0.0076
370 FS03 black
370 FS03 brown
c
% of summed alkanes >C20
n-alkane carbon chain length
HV-1 guano - p2 127 shots
HV-1 guano - p2 100 shots
HV-1 guano - p1 100 shots
r² = 0.79
p = 0.0001
HV-1 P2 100 shots
HV-1 P2 127 shots
r² = 0.53
p = 0.007
HV-1 P1 100 shots
HV-1 P2 127 shots

Figure 7.

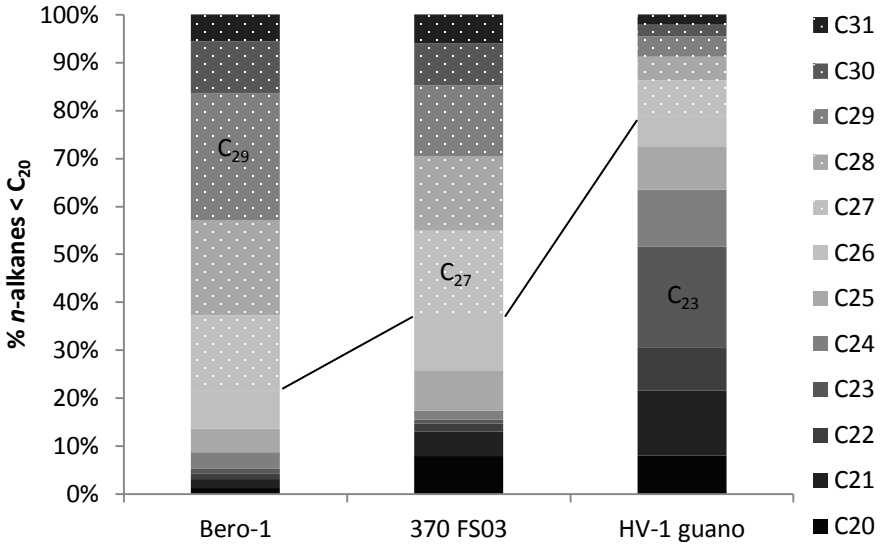
100%
90%
80%
70%
60%
50%
40%
30%
20%
10%
0%
% n-alkanes < C20
C29
C27
C23
Bero-1
370 FS03
HV-1 guano
C31
C30
C29
C28
C27
C26
C25
C24
C23
C22
C21
C20

Figure 8.

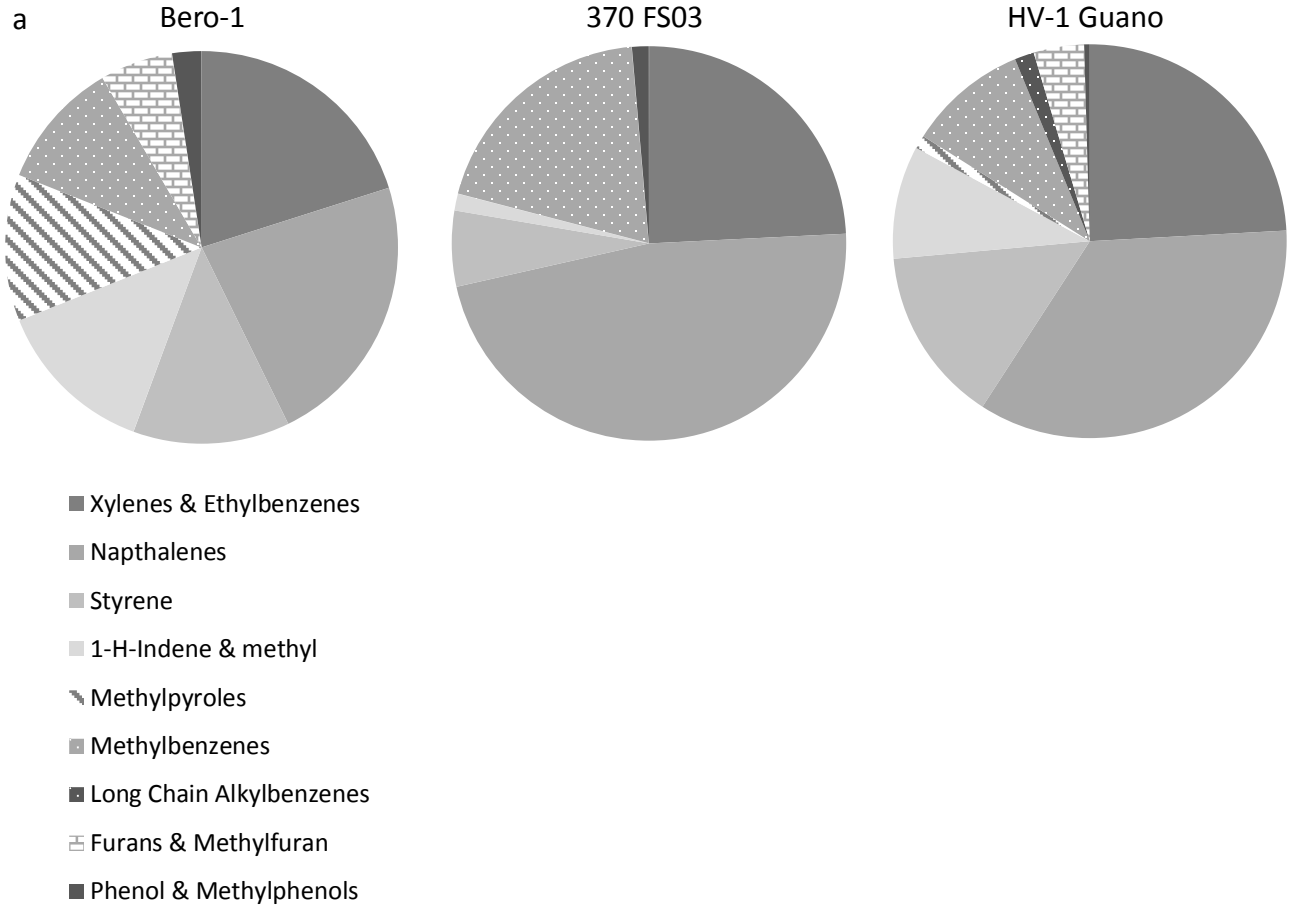
a
Bero-1
370 FS03
HV-1 Guano
Xylenes & Ethylbenzenes
Napthalenes
Styrene
1-H-Indene & methyl
Methylpyroles
Methylbenzenes
Long Chain Alkylbenzenes
Furans & Methylfuran
Phenol & Methylphenols

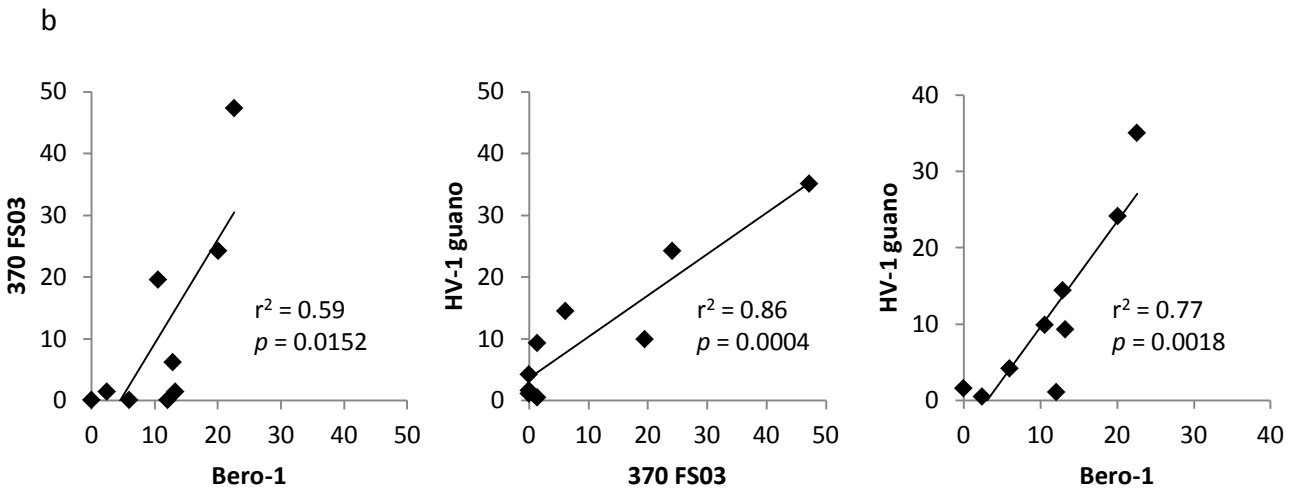
b
370 FS03
Bero-1
r² = 0.59
p = 0.0152
HV-1 guano
370 FS03
r² = 0.86
p = 0.0004
HV-1 guano
Bero-1
r² = 0.77
p = 0.0018

Figure 9.

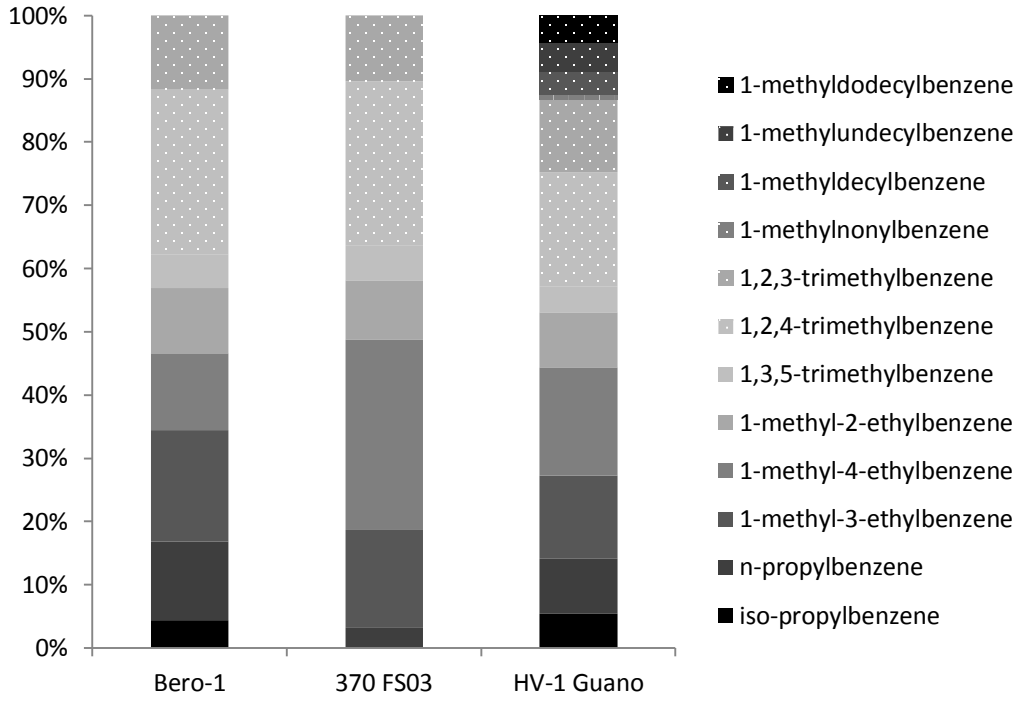
100%
90%
80%
70%
60%
50%
40%
30%
20%
10%
0%
Bero-1
370 FS03
HV-1 Guano
1-methyldodecylbenzene
1-methylundecylbenzene
1-methyldecylbenzene
1-methylnonylbenzene
1,2,3-trimethylbenzene
1,2,4-trimethylbenzene
1,3,5-trimethylbenzene
1-methyl-2-ethylbenzene
1-methyl-4-ethylbenzene
1-methyl-3-ethylbenzene
n-propylbenzene
iso-propylbenzene